Fluid Production Induced Stress Analysis Surrounding an Elliptic Fracture

by

Harshad Rajendra Pandit

A Thesis Presented in Partial Fulfillment

of the Requirements for the Degree

Master of Science

Approved November 2014 by the
Graduate Supervisory Committee:

Kangping Chen, Chair
Huei-Ping Huang
Marcus Herrmann

ARIZONA STATE UNIVERSITY

December 2014

ABSTRACT

Hydraulic fracturing is an effective technique used in well stimulation to increase petroleum well production. A combination of multi-stage hydraulic fracturing and horizontal drilling has led to the recent boom in shale gas production which has changed the energy landscape of North America.

During the fracking process, highly pressurized mixture of water and proppants (sand and chemicals) is injected into to a crack, which fractures the surrounding rock structure and proppants help in keeping the fracture open. Over a longer period, however, these fractures tend to close due to the difference between the compressive stress exerted by the reservoir on the fracture and the fluid pressure inside the fracture. During production, fluid pressure inside the fracture is reduced further which can accelerate the closure of a fracture.

In this thesis, we study the stress distribution around a hydraulic fracture caused by fluid production. It is shown that fluid flow can induce a very high hoop stress near the fracture tip. As the pressure gradient increases stress concentration increases. If a fracture is very thin, the flow induced stress along the fracture decreases, but the stress concentration at the fracture tip increases and become unbounded for an infinitely thin fracture.

The result from the present study can be used for studying the fracture closure problem, and ultimately this in turn can lead to the development of better proppants so that prolific well production can be sustained for a long period of time.

DEDICATION

To Aai, Baba, Ajoba

ACKNOWLEDGMENTS

I would like to express my heartfelt gratitude to my advisor and mentor: Dr. Kang Ping Chen for his support and guidance throughout this thesis project and my stay at ASU.

I am thankful to committee: Dr. Huei-Ping Huang and Dr. Marcus Herrmann, whose willingness to contribute their time, effort, and thoughtful consideration has made this thesis possible.

Finally, I am grateful to my family: Aai, Baba, and friends: Chetan, Koshik, Yogesh, Madhur, Sangram whose love and support continues to inspire me to pursue my goals.

TABLE OF CONTENTS

Page

LIST OF FIGURES

Figure Page

Figure Page

Figure Page

LIST OF SYMBOLS

Symbol Page

Symbol Page

CHAPTER 1

INTRODUCTION

Hydraulic fracturing has been widely used as a well stimulation method in petroleum engineering since 1940's. Hydraulically fractured wells have higher rate of well production. Hydraulic fracturing is one of the most important technologies behind the recent boom in shale gas production in North America. Because of the low emission rate of natural gas and the vast shale gas reserves in the US, advancement in hydraulic fracturing techniques is expected to continue to play a very important role in petroleum production for years to come.

There has been increased interest in studying fluid production mechanism from unconventional reservoirs such as shale where permeability is very low, often in the nano-darcy, and sometimes even in the sub-nano-darcy range. A related but less frequently studied issue is the closure of the hydraulic fractures over long times. Hydraulic fracturing in a shale involves horizontal wells and multiple fracturing. However, fluid production mechanisms and fracture closing mechanisms remain unchanged from those for a vertical fracture, which is much easier to analyze. Thus, the focus of the present work is on a single vertical fracture.

1.1 HYDRAULIC FRACTURING

Hydraulic fracturing also sometimes called as hydro-fracturing, hydro-fracking, fracking. It is a well-stimulation technique in which rock is fractured by a hydraulically pressurized liquid Fjaer et al (1992). Some hydraulic fractures form naturally. In this process highly pressurized mixture of water, proppants [1], chemicals are injected inside the well. As the resistance to flow in the formation increases, the pressure in the wellbore increases to a value that exceeds the breakdown pressure of the formation that is open to the wellbore. Once the formation 'breaks-down', a crack or fracture is formed, and the injected fluid begins moving down the fracture. The purpose of the propping agent is to prop open the fracture and keep the fracture open as shown in Figure 1.1.

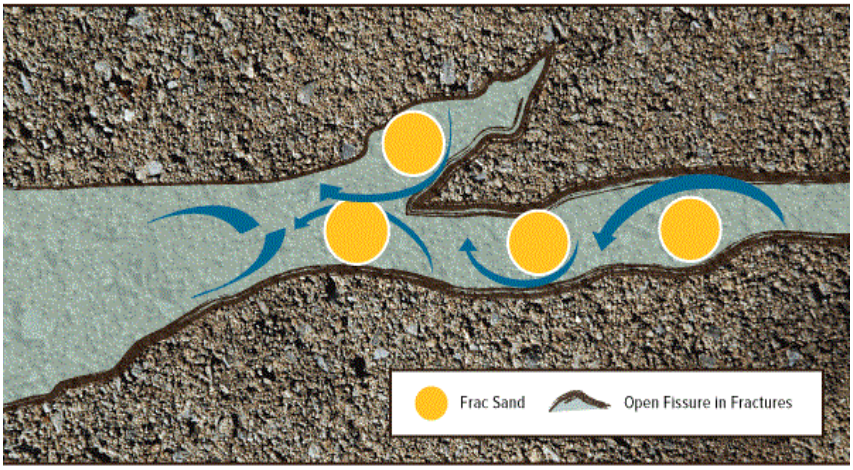

Figure 1.1 Fracking Proppants Holding the Fissure Open

(Source: http://www.forbes.com/sites/greatspeculations/2014/09/26/fracking-sand-among-the-best-pure-shale-plays/)

1.2 STRESSES IN A HYDRAULIC FRACTURING

Rocks at depth are subjected to stresses resulting from the weight of the overlying layers of rocks and from the stresses of geophysical origin. When a fracture is initiated in the rock, the stress field is locally disturbed and a new set of stresses are induced in the rock surrounding the fracture. Knowledge of the magnitudes and directions of these in situ and induced stresses is an essential component of underground fracturing process.

These in situ stresses are normally compressive, anisotropic, and nonhomogeneous as explained by Gidley et al (1989a) which means that the compressive stresses on the rock are not equal and vary in magnitude on the basis of direction. The magnitude and direction of the principal stresses are important because they control the pressure required to create and propagate a fracture, the shape of the fracture, the direction of the fracture, and the stresses trying to close the fracture.

Figure (1.2) shows the different pressures which needs to be considered during the fracking process.

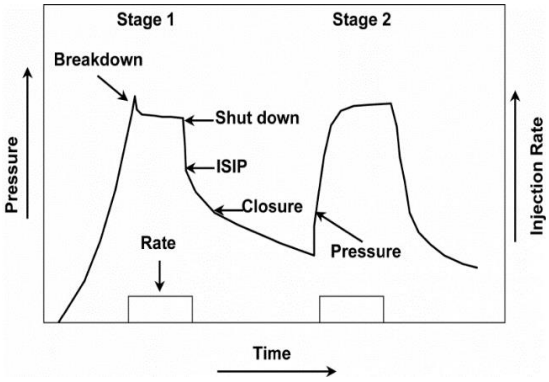

Figure 1.2 Different Types of Pressure in Fracking Process
(Source: http://petrowiki.org/Fracture_mechanics#cite_note-r2-1)

To initiate the Fracturing process, different fracture pressures needs to be considered. Breakdown pressure is the pressure needed to initiate a fracture in a rock. Closure pressure is the pressure at which the fracture closes after the fracturing pressure is relaxed. Both are determined by the overburden pressure, pore pressure, Poisson's Ratio, porosity and geophysical stresses.

Various studies have been done to study this closure stresses. The 2D circular arc crack solution was derived by Muskhelishvili (1953). It has been used widely to study curved crack behavior in an infinite, homogeneous and isotropic elastic material. Using this theory various numerical methods have been used to further analyze this solution. In the recent work by Elizabeth Ritz et al [2011] they have disproved the previous theory by Muskhelishvili. Many other studies have been done using different Numerical schemes Maiti S. K. et al (1997), Chow et al (1995) and different geometries of the fracture Sung Pil Heo et al (2002). All these studies on the closure stresses have been done keeping only in situ stresses and geophysical stresses into consideration Gidley et al (1989b), Sookprasong (1986), Sookprasong (2010), Montgomery et al (1984).

1.3 THESIS OVERVIEW

Stress induced by the fluid production process has never been considered for evaluating the closure stresses. This thesis proposes that the closure stress for a fracture can be significantly different from conventional estimate due to the addition of the flow induced stress. In light of the pressure gradient singularity present at the fracture tip

during fluid production Chen et al (2013), stress induced by fluid production can be important, particularly near the fracture tip. In Chapter 2, different factors affecting the fluid production is discussed. In Chapter 3, components of the flow induced stresses are being evaluated. The results are discussed in Chapter 4. Conclusions are made in Chapter 5.

CHAPTER 2

RESEARCH PROBLEM

Since the main focus of this thesis is to study the distribution of the flow-induced stress around a fracture, we will first discuss the pertinent parameters affecting the flow into a hydraulic fracture. To this end, we review the work of Prats (1961a) and Chen et al (2014) on the fluid production by a single elliptic fracture.

2.1 PRATS WORK

Past studies have shown that two flow regions are involved in fluid production from a hydraulically fractured wells (i) flow from the reservoir to the fracture, (ii) and flow along the length of the fracture from the tip to the well.

Prats (1961a) attributed the enhancement in the production of a fractured well to two main factors: large contact area between the fracture and the reservoir and the high conductivity pathway along the fracture, both of which are created during the fracturing process. Further analysis of these factors have been studied by Prats et al (1962), Gringarten et al (1975).

2.2 CHEN'S WORK

Recent study by Chen et al (2013) indicates that along with large contact area and high conductivity paths, there is one more significant factor enhancing the production rate

of a hydraulically fractured well. Chen has shown that the pressure gradient around the tip of the fracture is nearly singular, and it plays a major role in creating a large suction at the fracture tip, thus increasing the production rate of the fracture.

This near-singular suction force at the fracture tips makes production from unconventional reservoirs possible: with permeability down to nano-darcy, only a nearly-infinite suction force can move these fluids. He has also been able to show that the physical mechanism is broad and general and pressure gradient singularity exists regardless of the fracture conductivity.

2.3 PROBLEM SETUP

Studies on production from a fracture have considered different geometrical shapes for the fracture. Rounding off the sharp geometric ends of the fracture eliminates the singularity phenomenon mathematically. However, the reservoir pressure gradient still remains very large and near singular near the fracture ends, so long as the fracture is thin and long.

Prats has modelled the fracture as a degenerated ellipse in his work (1961b); and he has shown that elliptical geometry is more suitable for fracture related problems. For the same fracture area, a stronger but integrable singularity is always more beneficial to productivity. Modelling the fracture geometry by a nearly degenerate ellipse regularizes the pressure-gradient tip singularity. However, the pressure-gradient at the fracture tips

nevertheless remains very large and nearly singular. Hence we use degenerated ellipse for fracture in defining our problem.

In accordance with the previous work done by Chen et al (2014), Single fully-penetrated vertically-fractured well is considered with steady-state production. The fracture is modeled as a thin ellipse, which intersects the wellbore with a fracture width smaller than the wellbore diameter as shown in Figure 2.1. Assumption is made that the fracture conductivity is much higher than the reservoir conductivity so that the well production comes entirely from the fracture. The fracture length is considered much larger than the well radius so that the exit from the fracture to the well can be regarded as located at the y-axis.

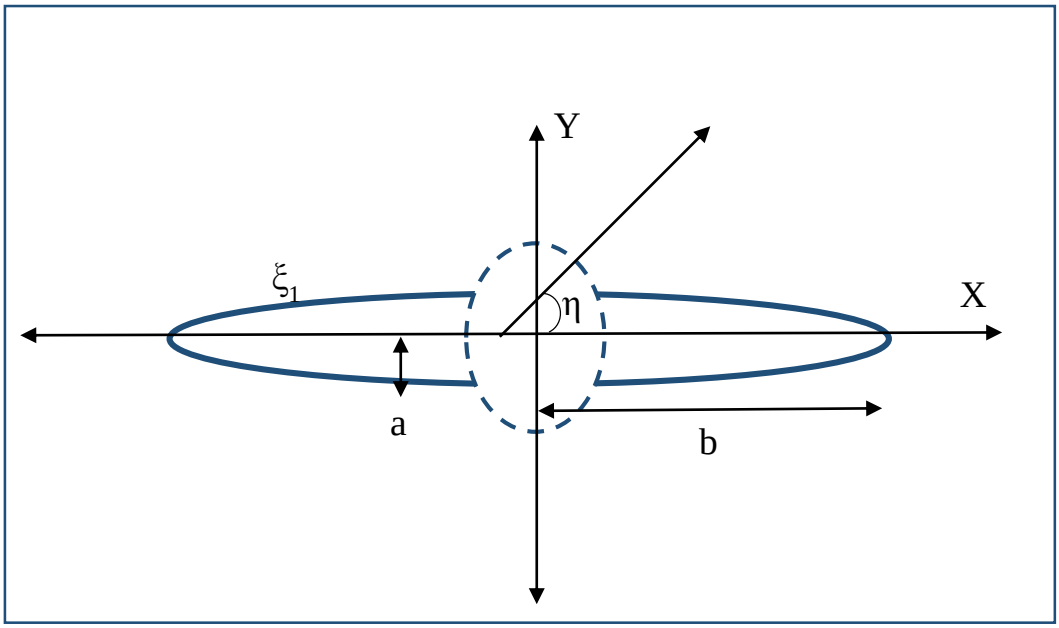

Figure 2.1 Top View of the Vertical Fracture

Where,$a = L\cosh\xi_1$, $b = L\sinh\xi_1$, L being the half crack length.

2.3.1 COORDINATE SYSTEM

Elliptical coordinate system is thus selected to study the problem at hand. To use elliptic system effectively, all the relevant mathematical operators are first expressed in this coordinate system.

Transformation equations from Cartesian coordinate to Elliptic coordinate are given by equation (2.1) and (2.2), and a graphical representation of the elliptic coordinate is shown in Figure 2.2:

$$X = L\ \cosh\xi\,.\cos\eta \tag{2.1}$$

$$Y = L\ \sinh\xi\,.\sin\eta \tag{2.2}$$

Where,

ξ is a non-negative real number

η ranges from 0 to 2π

L is half crack length

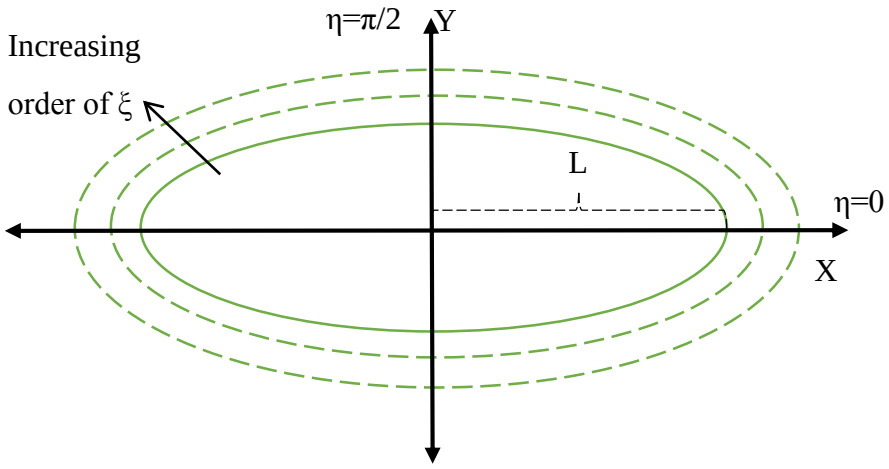

Fig 2.2 Elliptical Coordinate System

Constant ξ represents family of confocal ellipse, whereas constant η represents family of hyperbole as shown in Figure 2.3.

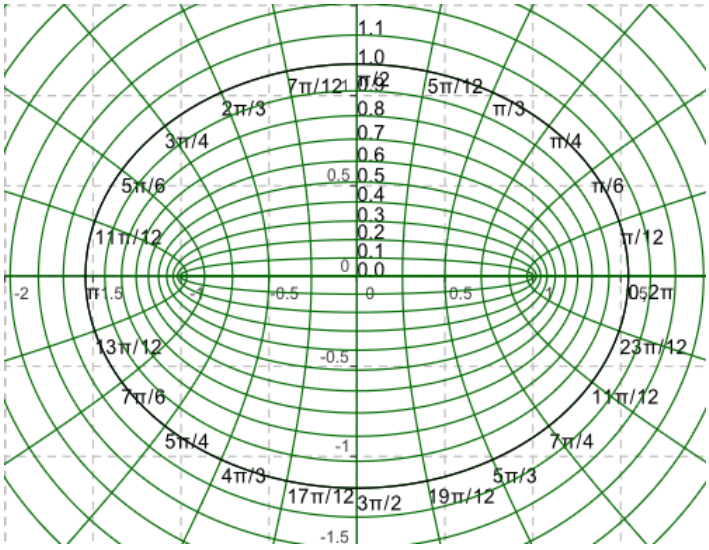

Figure 2.3. Family of Confocal Ellipse and Family of Hyperbole

(Source: "Elliptical coordinates grid" by SharkD - Own work. Licensed under Creative Commons Attribution-Share Alike 3.0-2.5-2.0-1.0 via Wikimedia Commons - http://commons.wikimedia.org/wiki/File:Elliptical_coordinates_grid.svg#mediaviewer/File:Elliptical_coordinates_grid.svg)

Position vector in elliptic coordinate system is represented as shown in Huston et al (2009)

$$\boldsymbol{P} = L\ \cosh\xi\,.\cos\eta\,\boldsymbol{n}_x + L\ \sinh\xi\,.\sin\eta\,\boldsymbol{n}_y \tag{2.3}$$

Where, $\boldsymbol{n}_x$ and $\boldsymbol{n}_y$ are unit vectors in X-direction and Y-direction respectively.

Base vectors are given by partially differentiating position vector with new coordinates at a time.

$$\frac{\partial \mathbf{P}}{\partial \xi} = \boldsymbol{g}_{\boldsymbol{\xi}} = L\ \sinh\xi\,.\cos\eta\,\boldsymbol{n}_x + L\ \cosh\xi\,.\sin\eta\,\boldsymbol{n}_y \tag{2.4}$$

$$\frac{\partial \boldsymbol{P}}{\partial \eta} = \boldsymbol{g}_{\boldsymbol{\eta}} = -L\ \cosh\xi\,.\sin\eta\,\boldsymbol{n}_x + L\ \sinh\xi\,.\cos\eta\,\boldsymbol{n}_y \tag{2.5}$$

Metric coefficients are then derived as the scalar dot product of base vectors as

$$g_{\xi\xi} = \mathrm{L}^2\,[\cosh 2\,\xi - \cos 2\,\eta] \tag{2.6}$$

$$g_{\eta\eta} = \mathrm{L}^2\,[\cosh 2\,\xi - \cos 2\,\eta] \tag{2.7}$$

Scale factors for any coordinate system are the most important property, as every other mathematical operators are primarily based on scale factors. Scale factors are square root of Matric coefficients. Hence scale factors for elliptic coordinate systems are defined as

$$h_1 = L\sqrt{[cosh^2\xi - cos^2\eta]} \tag{2.8}$$

$$h_2 = L\sqrt{[cosh^2\xi - cos^2\eta]} \tag{2.9}$$

Using these scale factors we can now easily define various differential operators in elliptic system.

Divergence of any vector in elliptic coordinate is given as

$$\nabla . \boldsymbol{F} = \frac{1}{h_1 . h_2}[\frac{\partial[h_2 . F_1]}{\partial\xi} + \frac{\partial[h_1 . F_2]}{\partial\eta}] \tag{2.10}$$

Where, **F** is any given vector with F_1 and F_2 being its components

Gradient of a Scalar in elliptic coordinate is given as

$$\nabla\mu = \frac{\hat{e}_1}{h_1}.\frac{\partial\mu}{\partial\xi} + \frac{\hat{e}_2}{h_2}.\frac{\partial\mu}{\partial\eta} \tag{2.11}$$

Where, μ is any given scalar and $\hat{e}_1$ and $\hat{e}_2$ being the unit vectors

Laplacian operator in elliptic coordinate is given as

$$\nabla^2\mu = \frac{1}{h_1.h_2}\left[\frac{\partial}{\partial\xi}\frac{h_2}{h_1}\frac{\partial}{\partial\xi} + \frac{\partial}{\partial\eta}\frac{h_1}{h_2}\frac{\partial}{\partial\eta}\right] \quad (2.12)$$

CHAPTER 3

STRESS ANALYSIS

To analyze the stress distribution in low permeable rocks, theory of poroelasticity needs to be considered. The general development of the linear poroelasticity was first given by Biot (1941). Biot's theory states that the isotropic, permeable porous rock, and the pore-filling fluid are in mechanical equilibrium. This theory gives a complete and general description of the mechanical behavior of a poroelastic medium. The evaluated stress in poroelastic media is always the effective stress.

If the pores of a poroelastic mass are filled with a fluid, and if a pressure is introduced into the pore fluid, it will try to separate the grains. This pressure is termed as pore pressure (p). The total compressive pressure caused by the surrounding is termed as the total stress. It is the combined effect of total stress and pore pressure that controls rock behavior such as shear strength, compression and distortion. The difference between the total stress and the pore pressure is called the effective stress as shown in Figure 3.1

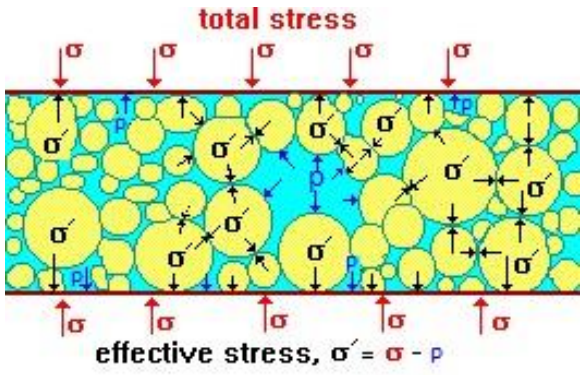

Figure 3.1 Effective Stress

(Source: http://environment.uwe.ac.uk/geocal/SoilMech/stresses/stresses.htm)

3.1 EQUILIBRIUM EQUATION

Now to study the effect of fluid production on the closure stresses, we will evaluate the stresses acting on and near the fracture due to this fluid production phenomenon.

Stress field are distributed continuously within a body due to distinctive body forces such as pressure gradient, gravitational forces due to weight, etc. For this problem related to crack in the rock, we will consider only the fluid pressure gradient, which in an elliptic coordinates is a body force $\nabla P(\xi,\eta)$ given by Chen et al (2014). For the porous rock under an equilibrium condition, all the forces are summed to zero:

$$\nabla.\sigma + \nabla P(\xi,\eta) = 0 \tag{3.1}$$

where, σ_{ij} is the stress tensor on the rock and the body force potential is the reservoir fluid pressure $P(\xi,\eta)$ given by Chen et. al. (2014):

$$P(\xi,\eta) = P_e + \Delta P.f\left\{\xi - \xi_e - \sum_{n=1}^{\infty}\frac{(-1)^n.\cos 2n\eta.\sinh 2n(\xi_e-\xi)}{n\cosh 2n(\xi_e-\xi_1)+n^2C_{fd}\sinh 2n(\xi_e-\xi_1)}\right\} \tag{3.2.1}$$

The components of the pressure gradient in the elliptic coordinate system are given by equations (3.2.2), (3.2.3):

$$\frac{\partial P(\xi,\eta)}{\partial \xi} = \frac{\Delta P.f}{h_1} + \sum_{n=1}^{\infty} \frac{\Delta P.f.2.(-1)^n.\cos 2n\eta.\cosh 2n(\xi_e - \xi)}{h_1\left(\cosh 2n(\xi_e - \xi_1) + nC_{fd}\sinh 2n(\xi_e - \xi_1)\right)} \quad (3.2.2)$$

$$\frac{\partial P(\xi,\eta)}{\partial \eta} = \sum_{n=1}^{\infty} \frac{\Delta P.f.2\,(-1)^n.\sin 2n\eta.\sinh 2n(\xi_e - \xi)}{h_2\left(\cosh 2n(\xi_e - \xi_1) + nC_{fd}\sinh 2n(\xi_e - \xi_1)\right)} \quad (3.2.3)$$

For further evaluations of the required terms, it is essential to find the second derivative of this pressure term with respect to ξ. This is shown in equation (3.2.4)

$$\frac{\partial^2 P(\xi,\eta)}{\partial \xi^2} = \frac{2.\Delta P.f.\sinh 2\xi}{L.\left[cosh^2\xi - cos^2\eta\right]^{\frac{3}{2}}} - \sum_{n=1}^{\infty} \frac{\Delta P.f.2.(-1)^n.\cos 2n\eta.\left(\cosh 2n\left(\xi_e - \xi\right).\frac{\partial h_1}{\partial \xi} + 2n.h_1.\sinh 2n\left(\xi_e - \xi\right)\right)}{{h_1}^2\left(\cosh 2n\left(\xi_e - \xi_1\right) + nC_{fd}\sinh 2n\left(\xi_e - \xi_1\right)\right)} \quad (3.2.4)$$

Where,

ξ_1 = Fracture Surface

ξ_e = Outer Boundary of Reservoir

P_e = Far Field Pressure

P_w = Pressure at the fracture exit to the well

$\Delta P = P_e - P_w$ (Pressure drawdown)

C_{fd} = Dimensionless Fracture Conductivity

$$C_{fd} = \frac{K_f w_f}{K_m L}$$

K_f = Permeability of Fracture

K_m = Permeability of Reservoir

w_f = the aperture of the fracture at the well

The term 'f' has been defined as a function of C_{fd}, ξ_1, ξ_e by Chen as follows

$$f = \frac{1}{\xi_e - \xi_1 + \frac{1}{C_{fd}}\left[\frac{\pi^2}{6} - \sum_{n=1}^{\infty} \frac{1}{n^2 + n^3 C_{fd} \tanh 2n(\xi_e - \xi_1)}\right]} \quad (3.3.1)$$

For the case where the fracture conductivity is large, which corresponds to the situation where the pressure loss along the fracture is small, f can be further simplified. For the limit of large ξ_e, small ξ_1 and large values of C_{fd}, we can approximate the function f as

$$f = \frac{1}{\xi_e - \frac{\pi^2}{6C_{fd}}} \quad (3.3.2)$$

The two terms in the bracket of (3.2.1) shows that the flow in the reservoir is due to the superposition of two basic flows:

- Confocal elliptical flow
- Redistributive non-producing flow

Using (2.10) and (2.11), the equilibrium equation (3.1) in elliptic coordinate can be written as

$$\frac{\partial\left[h_2.\sigma_{\xi\xi}\right]}{\partial\xi}+\frac{\partial\left[h_1.\sigma_{\xi\eta}\right]}{\partial\eta}+\sigma_{\xi\eta}\frac{\partial h_1}{\partial\eta}-\sigma_{\eta\eta}\frac{\partial h_2}{\partial\eta}+\frac{\hat{\mathrm{e}}_1}{h_1}.\frac{\partial P}{\partial\xi}=0 \tag{3.4.1}$$

$$\frac{\partial\left[h_2.\sigma_{\xi\eta}\right]}{\partial\xi}+\frac{\partial\left[h_1.\sigma_{\eta\eta}\right]}{\partial\eta}+\sigma_{\xi\eta}\frac{\partial h_2}{\partial\eta}-\sigma_{\xi\xi}\frac{\partial h_2}{\partial\eta}+\frac{\hat{\mathrm{e}}_2}{h_2}.\frac{\partial P}{\partial\eta}=0 \tag{3.4.2}$$

3.2 STRESS FUNCTION

The equilibrium equations (3.4.1), (3.4.2) are very difficult to solve direct using analytical method. However, a scalar potential function Φ called Airy stress function can be used to the solution. The Airy stress function is a special form of the Beltrami stress function. This special type of stress function is specifically used in two-dimensional space. In general, when a stress function is used to solve the static governing equation, the stress function satisfies the governing equation only if the body force is conservative, possessing a body force potential. In our problem, the body force potential is clearly the reservoir fluid pressure.

Stress functions are in general defined by the relations as shown in Coker et al (1957),

$$\sigma_x = \frac{\partial^2 \Phi}{\partial y^2}, \qquad \sigma_y = \frac{\partial^2 \Phi}{\partial x^2}, \qquad \sigma_{xy} = -\frac{\partial^2 \Phi}{\partial x \partial y} \tag{3.5.1}$$

In order to determine the constraints placed on the stress function, the compatibility equation needs to be considered. Using the definition of the stress function, we can show that the compatibility equation is automatically satisfied. The equilibrium equation gives

$$\frac{\partial^4 \Phi}{\partial x^4} + 2\frac{\partial^4 \Phi}{\partial x^2 \partial y^2} + \frac{\partial^4 \Phi}{\partial y^4} = \left(\frac{\partial^2}{\partial x^4} + \frac{\partial^2}{\partial y^2}\right)^2 \Phi = 0 \tag{3.5.2}$$

$$\nabla^4 \Phi = 0$$

This shows that the stress function must be biharmonic in nature. This system of stress function can also be extended to the cases where body force is non-zero, provided that the body force is expressed in terms of gradient of scalar potential which is the reservoir pressure for our case. Thus applying operators in elliptical coordinates to equilibrium equations, we get stress equilibrium equation in elliptic coordinate system. After expressing this stress equilibrium equation in terms of stress function and simplifying as per Coker et al (1957) we then obtain the stress components as

$$\sigma_{\xi\xi} = \frac{1}{2J^2}\frac{\partial^2\Phi}{\partial\eta^2} + \frac{1}{(2J^2)^2}\frac{\partial\Phi}{\partial\xi}\frac{\partial(2J^2)}{\partial\xi} - \frac{1}{(2J^2)^2}\frac{\partial\Phi}{\partial\eta}\frac{\partial(2J^2)}{\partial\eta} + P(\xi,\eta) \tag{3.6.1}$$

$$\sigma_{\eta\eta} = \frac{1}{2J^2}\frac{\partial^2\Phi}{\partial\xi^2} + \frac{1}{(2J^2)^2}\frac{\partial\Phi}{\partial\eta}\frac{\partial(2J^2)}{\partial\eta} - \frac{1}{(2J^2)^2}\frac{\partial\Phi}{\partial\xi}\frac{\partial(2J^2)}{\partial\xi} + P(\xi,\eta) \tag{3.6.2}$$

$$\sigma_{\xi\eta} = -\frac{1}{2J^2}\frac{\partial^2\Phi}{\partial\xi\partial\eta} + \frac{1}{(2J^2)^2}\frac{\partial\Phi}{\partial\xi}\frac{\partial(2J^2)}{\partial\eta} + \frac{1}{(2J^2)^2}\frac{\partial\Phi}{\partial\eta}\frac{\partial(2J^2)}{\partial\xi} \tag{3.6.3}$$

Where,

$$(2J^2) = L^2(\cosh 2\xi - \cos 2\eta) \tag{3.7}$$

Equation (3.6.1), (3.6.2), (3.6.3) simplifies to

$$\sigma_{\xi\xi} = \frac{1}{2J^2}\frac{\partial^2\Phi}{\partial\eta^2} + \frac{L^2\sinh 2\xi}{(2J^2)^2}\frac{\partial\Phi}{\partial\xi} - \frac{L^2\sin 2\eta}{(2J^2)^2}\frac{\partial\Phi}{\partial\eta} + P(\xi,\eta) \tag{3.8.1}$$

$$\sigma_{\eta\eta} = \frac{1}{2J^2}\frac{\partial^2\Phi}{\partial\xi^2} + \frac{L^2\sin 2\eta}{(2J^2)^2}\frac{\partial\Phi}{\partial\eta} - \frac{L^2\sinh 2\xi}{(2J^2)^2}\frac{\partial\Phi}{\partial\xi} + P(\xi,\eta) \tag{3.8.2}$$

$$\sigma_{\xi\eta} = -\frac{1}{2J^2}\frac{\partial^2 \Phi}{\partial\xi\partial\eta} + \frac{L^2 \sin 2\eta}{(2J^2)^2}\frac{\partial \Phi}{\partial\xi} + \frac{L^2 \sinh 2\xi}{(2J^2)^2}\frac{\partial \Phi}{\partial\eta} \tag{3.8.3}$$

To find the final expressions for the stress components, we must find the stress function Φ. Solution for Φ is assumed to be a linear combination of the 10 solutions listed below, which are fundamental solutions of the biharmonic equation, as per Coker et al (1957).

The biharmonic equation solution $\nabla^4 \Phi = 0$ gives four independent solutions,

$$\Phi_1 = e^{(n+1)\xi}\cos(n-1)\eta + e^{(n-1)\xi}\cos(n+1)\eta \tag{3.9.1}$$

$$\Phi_2 = e^{-(n+1)\xi}\cos(n-1)\eta + e^{-(n-1)\xi}\cos(n+1)\eta \tag{3.9.2}$$

$$\Phi_3 = e^{(n+1)\xi}\sin(n-1)\eta + e^{(n-1)\xi}\sin(n+1)\eta \tag{3.9.3}$$

$$\Phi_4 = e^{-(n+1)\xi}\sin(n-1)\eta + e^{-(n-1)\xi}\sin(n+1)\eta \tag{3.9.4}$$

We also have four different harmonic functions in the form of

$$\Phi_5 = e^{n\xi} \cos n\eta \tag{3.9.5}$$

$$\Phi_6 = e^{-n\xi} \cos n\eta \tag{3.9.6}$$

$$\Phi_7 = e^{n\xi} \sin n\eta \tag{3.9.7}$$

$$\Phi_8 = e^{-n\xi} \cos n\eta \tag{3.9.8}$$

In addition, there are two special harmonic solutions,

$$\Phi_9 = \xi \tag{3.9.9}$$

$$\Phi_{10} = \eta \tag{3.9.10}$$

In the above, ‘n’ is any non-zero real number. All of these10 functions can combined to provide us a general solution for the stress function.

$$\Phi = A_0\xi + B_0\eta + C_n\left[e^{(n+1)\xi}\cos(n-1)\eta + e^{(n-1)\xi}\cos(n+1)\eta\right] \quad (3.10)$$
$$+ D_n\left[e^{-(n+1)\xi}\cos(n-1)\eta + e^{-(n-1)\xi}\cos(n+1)\eta\right]$$
$$+ E_n\left[e^{(n+1)\xi}\sin(n-1)\eta + e^{(n-1)\xi}\sin(n+1)\eta\right]$$
$$+ F_n\left[e^{-(n+1)\xi}\sin(n-1)\eta + e^{-(n-1)\xi}\sin(n+1)\eta\right]$$
$$+ G_n\left[e^{n\xi}\cos n\eta\right] + H_n\left[e^{-n\xi}\cos n\eta\right] + I_n\left[e^{n\xi}\sin n\eta\right]$$
$$+ J_n[e^{-n\xi}\sin n\eta]$$

Using these function, different stress component values were evaluated. For example, assuming n=1 for Φ_1, Φ_2, Φ_3, Φ_4, Φ_7, Φ_8, Φ_9, Φ_{10}, and n=2 for Φ_5, Φ_6, we have:

Values of $\sigma_{\xi\xi}$are as follows

$$L^2(\cosh 2\xi - \cos 2\eta)^2\sigma_{\xi\xi 1} \quad (3.11.1)$$
$$= 2\cos 4\eta - 8\cos 2\eta\cosh 2\xi + 4 + 2e^{4\xi}$$

$$L^2(\cosh 2\xi - \cos 2\eta)^2\sigma_{\xi\xi 2} \quad (3.11.2)$$
$$= 2\cos 4\eta - 8\cos 2\eta\cosh 2\xi + 4 + 2e^{-4\xi}$$

$$L^2(\cosh 2\xi - \cos 2\eta)^2 \sigma_{\xi\xi 3} = 2\sin 4\eta - 8\sin 2\eta \cosh 2\xi \tag{3.11.3}$$

$$L^2(\cosh 2\xi - \cos 2\eta)^2 \sigma_{\xi\xi 4} = 2\sin 4\eta - 8\sin 2\eta \cosh 2\xi \tag{3.11.4}$$

$$L^2(\cosh 2\xi - \cos 2\eta)^2 \sigma_{\xi\xi 5} \tag{3.11.5}$$
$$= \cos 4\eta e^{2\xi} - \cos 2\eta e^{4\xi} + 3\cos 2\eta + 3e^{2\xi}$$

$$L^2(\cosh 2\xi - \cos 2\eta)^2 \sigma_{\xi\xi 6} \tag{3.11.6}$$
$$= \cos 4\eta e^{-2\xi} - \cos 2\eta e^{-4\xi} + 3\cos 2\eta + 3e^{-2\xi}$$

$$L^2(\cosh 2\xi - \cos 2\eta)^2 \sigma_{\xi\xi 7} \tag{3.11.7}$$
$$= \sin 4\eta\, e^{2\xi} - \sin 2\eta e^{4\xi} - 3\sin 2\eta$$

$$L^2(\cosh 2\xi - \cos 2\eta)^2 \sigma_{\xi\xi 8} \tag{3.11.8}$$
$$= \sin 4\eta\, e^{-2\xi} - \sin 2\eta e^{-4\xi} - 3\sin 2\eta$$

$$L^2(\cosh 2\xi - \cos 2\eta)^2 \sigma_{\xi\xi 9} = 2\sinh 2\xi \tag{3.11.9}$$

$$L^2(\cosh 2\xi - \cos 2\eta)^2 \sigma_{\xi\xi 10} = -2\sin 2\eta \tag{3.11.10}$$

Values of $\sigma_{\eta\eta}$ are as follows

$$L^2(\cosh 2\xi - \cos 2\eta)^2 \sigma_{\eta\eta 1} \tag{3.12.1}$$
$$= 2\cos 4\eta - 8\cos 2\eta\, e^{2\xi} + 4 + 2e^{4\xi}$$

$$L^2(\cosh 2\xi - \cos 2\eta)^2 \sigma_{\eta\eta 2} \tag{3.12.2}$$
$$= 2\cos 4\eta - 8\cos 2\eta\, e^{-2\xi} + 4 + 2e^{-4\xi}$$

$$L^2(\cosh 2\xi - \cos 2\eta)^2 \sigma_{\eta\eta 3} = 2\sin 4\eta \tag{3.12.3}$$

$$L^2(\cosh 2\xi - \cos 2\eta)^2 \sigma_{\eta\eta 4} = 2\sin 4\eta \tag{3.12.4}$$

$$L^2(\cosh 2\xi - \cos 2\eta)^2\sigma_{\eta\eta 5} \tag{3.12.5}$$
$$= -\cos 4\eta e^{2\xi} + \cos 2\eta e^{4\xi} - 3\cos 2\eta - 3e^{2\xi}$$

$$L^2(\cosh 2\xi - \cos 2\eta)^2\sigma_{\eta\eta 6} \tag{3.12.6}$$
$$= -\cos 4\eta e^{-2\xi}$$
$$+ \cos 2\eta e^{-4\xi} - 3\cos 2\eta - 3e^{-2\xi}$$

$$L^2(\cosh 2\xi - \cos 2\eta)^2\sigma_{\eta\eta 7} \tag{3.12.7}$$
$$= -\sin 4\eta\, e^{2\xi} + \sin 2\eta e^{4\xi} + 3\sin 2\eta$$

$$L^2(\cosh 2\xi - \cos 2\eta)^2\sigma_{\eta\eta 8} \tag{3.12.8}$$
$$= -\sin 4\eta\, e^{-2\xi} + \sin 2\eta e^{-4\xi} + 3\sin 2\eta$$

$$L^2(\cosh 2\xi - \cos 2\eta)^2\sigma_{\eta\eta 9} = -2\sinh 2\xi \tag{3.12.9}$$

$$L^2(\cosh 2\xi - \cos 2\eta)^2\sigma_{\eta\eta 10} = 2\sin 2\eta \tag{3.12.10}$$

Values of $\sigma_{\xi\eta}$are as follows

$$L^2(\cosh 2\xi - \cos 2\eta)^2\sigma_{\xi\eta 1} = 4\sin 2\eta \cosh 2\xi \tag{3.13.1}$$

$$L^2(\cosh 2\xi - \cos 2\eta)^2\sigma_{\xi\eta 2} = -4\sin 2\eta \cosh 2\xi \tag{3.13.2}$$

$$L^2(\cosh 2\xi - \cos 2\eta)^2\sigma_{\xi\eta 3} = 4\cos 2\eta \sinh 2\xi \tag{3.13.3}$$

$$L^2(\cosh 2\xi - \cos 2\eta)^2\sigma_{\xi\eta 4} = -4\cos 2\eta \sinh 2\xi \tag{3.13.4}$$

$$L^2(\cosh 2\xi - \cos 2\eta)^2\sigma_{\xi\eta 5} \tag{3.13.5}$$
$$= -\sin 4\eta e^{2\xi} + \sin 2\eta e^{4\xi} + 3\sin 2\eta$$

$$L^2(\cosh 2\xi - \cos 2\eta)^2\sigma_{\xi\eta 6} \tag{3.13.6}$$
$$= \sin 4\eta e^{-2\xi} - \sin 2\eta e^{-4\xi} - 3\sin 2\eta$$

$$L^2(\cosh 2\xi - \cos 2\eta)^2\sigma_{\xi\eta 7} \tag{3.13.7}$$
$$= \cos 4\eta e^{2\xi} - \cos 2\eta e^{4\xi} - 3\cos 2\eta$$

$$L^2(\cosh 2\xi - \cos 2\eta)^2 \sigma_{\xi\eta 8} = \cos 4\eta e^{-2\xi} + \cos 2\eta e^{-4\xi} + 3\cos 2\eta \quad (3.13.8)$$

$$L^2(\cosh 2\xi - \cos 2\eta)^2 \sigma_{\xi\eta 9} = 2\sin 2\eta \quad (3.13.9)$$

$$L^2(\cosh 2\xi - \cos 2\eta)^2 \sigma_{\xi\eta 10} = 2\sinh 2\xi \quad (3.13.10)$$

Applying boundary conditions to (3.10), and selecting appropriate function from (3.11), (3.12) & (3.13) we can find the stress function for the problem considered.

3.3 BOUNDARY CONDITIONS

To find the stresses in the given domain, certain boundary conditions must be applied. Boundary condition on the fracture surface for the normal stress in ξ direction is straight forward: it equals the negative of the internal pressure in the fracture, which is given by Chen et al (2014):

$$P_{f(\eta)} = P_w + \frac{\Delta P}{C_{fd}} . f \left\{ \frac{\pi^2}{4} - \eta^2 - \sum_{n=1}^{\infty} \frac{(-1)^{2n} - (-1)^n \cos 2n\eta}{n^2 + n^3 C_{fd} \tanh 2n(\xi_e - \xi_1)} \right\} \quad (3.14)$$

This boundary condition is graphically shown in Figure 3.2.

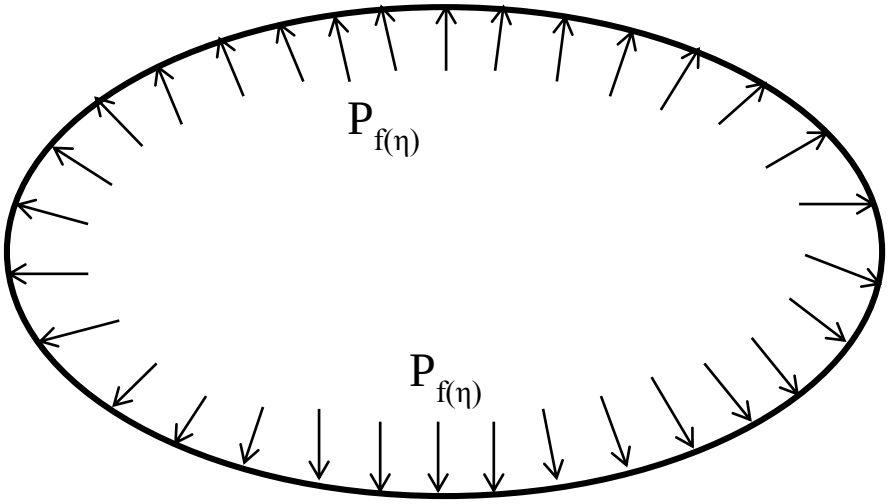

Fig 3.2 Boundary Condition at ξ_1 , All Round Tension $P_{f(\eta)}$

To find the shear stress $\sigma_{\xi\eta}$ at the fracture surface, consider an infinitesimally small section of the fracture boundary as shown in Fig 3.3

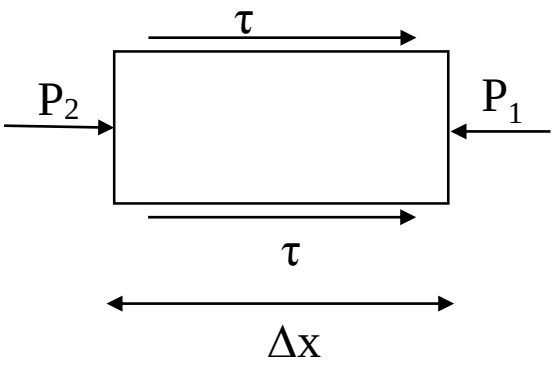

Fig 3.3 Shear Stress Condition at the Fracture Boundary

Consider the case where P1 > P2.

$$\tau = \frac{Area}{Circumference} . \frac{P_1 - P_2}{\Delta x}$$

$$(Circumference . \Delta x) . \tau = (P_1 - P_2) . Area$$

$$\tau = \frac{Area}{Circumference} . \frac{dP}{\Delta x} \qquad (3.15)$$

$$\tau = \frac{\partial P_f}{\partial \eta}$$

Since the stresses considered are ‘flow-induced’, at the far boundary, all the stresses are set to be zero. All the boundary conditions are listed below:

$$At\ \xi = \xi_1,$$

$$\sigma_{\xi\xi} = P_f \tag{3.16.1}$$

$$\sigma_{\xi\eta} = \frac{\partial P_f}{\partial \eta} \tag{3.16.2}$$

$$At\ \xi = \xi_e,$$

$$\sigma_{\xi\xi} = 0 \tag{3.16.3}$$

$$\sigma_{\eta\eta} = 0 \tag{3.16.4}$$

$$\sigma_{\xi\eta} = 0 \tag{3.16.5}$$

Second boundary condition (3.16.2) is given by taking the gradient of the reservoir pressure term in η direction:

$$\frac{\partial P_f}{\partial \eta} = -\frac{2.\Delta P.f.\eta}{C_{fd}} - \frac{\Delta P.f}{C_{fd}} \sum_{n=1}^{\infty} \frac{2(-1)^n \sin 2n\eta}{n + n^2 C_{fd} \tanh 2n(\xi_e - \xi_1)} \tag{3.17.1}$$

For further use, we may also evaluate the partial derivative of (3.17.1):

$$\frac{\partial^2 P_f}{\partial \eta^2} = -\frac{2.\Delta P.f}{C_{fd}} - \frac{\Delta P.f}{C_{fd}} \sum_{n=1}^{\infty} \frac{4(-1)^n \cos 2n\eta}{1 + nC_{fd} \tanh 2n(\xi_e - \xi_1)} \quad (3.17.2)$$

Far end boundary conditions are given by third, fourth and fifth boundary condition which stats that normal stresses in ξ direction ($\sigma_{\xi\xi}$) and η ($\sigma_{\eta\eta}$) direction and shear stress $\sigma_{\xi\eta}$ are all zero.

3.4 STRESS VALUES

Analyzing the terms involved in boundary conditions, only related Stress Function solutions were selected. They were as follows

$$\Phi_{\mathrm{A}} = e^{2\xi} + \cos 2\eta \quad (3.18.1)$$

$$\Phi_{\mathrm{B}} = e^{-2\xi} + \cos 2\eta \quad (3.18.2)$$

$$\Phi_{\mathrm{E}} = e^{2\xi} \cos 2\eta \quad (3.18.3)$$

$$\Phi_{\mathrm{F}} = e^{-2\xi} \cos 2\eta \quad (3.18.4)$$

$$\Phi_{\mathrm{I}} = \xi \quad (3.18.5)$$

This leaves us with the general solution of stress function in the form of

$$\Phi = \mathrm{A}\left[e^{2\xi} + \cos 2\eta\right] + \mathrm{B}\left[e^{-2\xi} + \cos 2\eta\right] + \mathrm{E}\left[e^{2\xi}\cos 2\eta\right] + \mathrm{F}\left[e^{-2\xi}\cos 2\eta\right] + \mathrm{I}\xi \tag{3.19}$$

Using the Boundary Conditions from equation (3.16.1) through equation (3.16.5) coefficients for the equation (3.19) were evaluated as follows

$$\mathrm{A} = -4\sinh(2\xi_e)\cosh(2\xi_1) \tag{3.20.1}$$

$$B = 4\sinh(2\xi_e)\cosh(2\xi_1) \tag{3.20.2}$$

$$E = 2\sinh(2\xi_e)\,e^{4\xi_e}(\cosh(2\xi_e) + \cosh(2\xi_1)) - 4sinh^2(2\xi_e)e^{2\xi_e} \tag{3.20.3}$$

$$F = -2\sinh(2\xi_e)\left[\cosh(2\xi_e) + \cosh(2\xi_1) + 2\sinh(2\xi_e)\,e^{-2\xi_e}\right] \tag{3.20.4}$$

$$I = 2\sinh(2\xi_e) \tag{3.20.5}$$

Thus using these coefficients, we get Stress Function Φ as

$$\begin{aligned}\Phi = {} & -4\sinh(2\xi_e)\cosh(2\xi_1)\left[e^{2\xi} + \cos 2\eta\right] \\ & + 4\sinh(2\xi_e)\cosh(2\xi_1)\left[e^{-2\xi} + \cos 2\eta\right] \\ & + 2\sinh(2\xi_e)\, e^{4\xi_e}(\cosh(2\xi_e) + \cosh(2\xi_1)) \\ & - 4sinh^2(2\xi_e)e^{2\xi_e}\left[e^{2\xi}\cos 2\eta\right] \\ & - 2\sinh(2\xi_e)\left[\cosh(2\xi_e) + \cosh(2\xi_1)\right. \\ & \left. + 2\sinh(2\xi_e)\, e^{-2\xi_e}\right]\left[e^{-2\xi}\cos 2\eta\right] + 2\sinh(2\xi_e)\,\xi\end{aligned} \tag{3.21}$$

Using this solution for Stress Function in equation (3.8.1), (3.8.2), (3.8.3) $\sigma_{\xi\xi}$, $\sigma_{\eta\eta}$, $\sigma_{\xi\eta}$ are evaluated as shown below

$$\sigma_{\xi\xi} = \frac{1}{(\cosh 2\xi - \cos 2\eta)}\Big[\{2\,e^{4\xi_e}\sinh(2\xi_e)(\cosh(2\xi_e) + \cosh(2\xi_1)) \tag{3.22.1}$$

$$- 4e^{2\xi_e}sinh^2(2\xi_e)\}4e^{2\xi}\cos 2\eta$$

$$-\{2\sinh(2\xi_e)(\cosh(2\xi_e) + \cosh(2\xi_1))$$

$$- 2e^{-2\xi_e}sinh^2(2\xi_e)\}4e^{-2\xi}\cos 2\eta\Big]$$

$$+\frac{\sinh 2\xi}{(\cosh 2\xi - \cos 2\eta)^2}\Big[8\sinh(2\xi_e)\cosh(2\xi_1)\big(e^{2\xi}$$

$$+ e^{-2\xi}\big)$$

$$+\{2\,e^{4\xi_e}\sinh(2\xi_e)(\cosh(2\xi_e) + \cosh(2\xi_1))$$

$$- 4e^{2\xi_e}sinh^2(2\xi_e)\}2e^{2\xi}\cos 2\eta$$

$$+\{2\sinh(2\xi_e)(\cosh(2\xi_e) + \cosh(2\xi_1))$$

$$- 2e^{-2\xi_e}sinh^2(2\xi_e)\}2e^{-2\xi}\cos 2\eta + 2\sinh(2\xi_e)\Big]$$

$$-\frac{\sin 2\eta}{(\cosh 2\xi - \cos 2\eta)^2}\Big[-\{2\,e^{4\xi_e}\sinh(2\xi_e)(\cosh(2\xi_e)$$

$$+\cosh(2\xi_1)) - 4e^{2\xi_e}sinh^2(2\xi_e)\}2e^{2\xi}\sin 2\eta$$

$$+\{2\sinh(2\xi_e)(\cosh(2\xi_e) + \cosh(2\xi_1))$$

$$- 2e^{-2\xi_e}sinh^2(2\xi_e)\}2e^{-2\xi}\sin 2\eta\Big] + P(\xi,\eta)$$

$\sigma_{\eta\eta}$ (3.22.2)

$$= \frac{1}{(\cosh 2\xi - \cos 2\eta)}\left[16\sinh(2\xi_e)\cosh(2\xi_1)e^{-2\xi}\left(e^{4\xi}-1\right)\right.$$

$$+\left\{2\,e^{4\xi_e}\sinh(2\xi_e)(\cosh(2\xi_e)+\cosh(2\xi_1))\right.$$

$$\left.-4e^{2\xi_e}sinh^2(2\xi_e)\right\}4e^{2\xi}\cos 2\eta$$

$$-\left\{2\sinh(2\xi_e)(\cosh(2\xi_e)+\cosh(2\xi_1))\right.$$

$$\left.-2e^{-2\xi_e}sinh^2(2\xi_e)\right\}4e^{-2\xi}\cos 2\eta\Big]$$

$$+\frac{\sin 2\eta}{(\cosh 2\xi - \cos 2\eta)^2}\left[8\sinh(2\xi_e)\cosh(2\xi_1)\left(e^{2\xi}+e^{-2\xi}\right)\right.$$

$$+\left\{2\,e^{4\xi_e}\sinh(2\xi_e)(\cosh(2\xi_e)+\cosh(2\xi_1))\right.$$

$$\left.-4e^{2\xi_e}sinh^2(2\xi_e)\right\}2e^{2\xi}\cos 2\eta$$

$$+\left\{2\sinh(2\xi_e)(\cosh(2\xi_e)+\cosh(2\xi_1))\right.$$

$$\left.-2e^{-2\xi_e}sinh^2(2\xi_e)\right\}2e^{-2\xi}\cos 2\eta+2\sinh(2\xi_e)\Big]$$

$$-\frac{\sinh 2\xi}{(\cosh 2\xi - \cos 2\eta)^2}\left[-\left\{2\,e^{4\xi_e}\sinh(2\xi_e)(\cosh(2\xi_e)+\cosh(2\xi_1))\right.\right.$$

$$\left.-4e^{2\xi_e}sinh^2(2\xi_e)\right\}2e^{2\xi}\sin 2\eta$$

$$+\left\{2\sinh(2\xi_e)(\cosh(2\xi_e)+\cosh(2\xi_1))\right.$$

$$\left.-2e^{-2\xi_e}sinh^2(2\xi_e)\right\}2e^{-2\xi}\sin 2\eta\Big]+P(\xi,\eta)$$

$$\sigma_{\xi\eta} \tag{3.22.3}$$

$$= -\frac{1}{(\cosh 2\xi - \cos 2\eta)}\Big[-\big\{2\,e^{4\xi_e}\sinh(2\xi_e)(\cosh(2\xi_e)$$

$$+ \cosh(2\xi_1)) - 4e^{2\xi_e}sinh^2(2\xi_e)\big\}4e^{2\xi}\cos 2\eta$$

$$+ \big\{2\sinh(2\xi_e)(\cosh(2\xi_e) + \cosh(2\xi_1))$$

$$- 2e^{-2\xi_e}sinh^2(2\xi_e)\big\}4e^{-2\xi}\cos 2\eta\Big]$$

$$+ \frac{\sin 2\eta}{(\cosh 2\xi - \cos 2\eta)^2}\Big[-\big\{2\,e^{4\xi_e}\sinh(2\xi_e)(\cosh(2\xi_e) + \cosh(2\xi_1))$$

$$- 4e^{2\xi_e}sinh^2(2\xi_e)\big\}2e^{2\xi}\sin 2\eta$$

$$+ \big\{2\sinh(2\xi_e)(\cosh(2\xi_e) + \cosh(2\xi_1))$$

$$- 2e^{-2\xi_e}sinh^2(2\xi_e)\big\}2e^{-2\xi}\sin 2\eta\Big]$$

$$+ \frac{\sinh 2\xi}{(\cosh 2\xi - \cos 2\eta)^2}\Big[8\sinh(2\xi_e)\cosh(2\xi_1)\big(e^{2\xi} + e^{-2\xi}\big)$$

$$+ \big\{2\,e^{4\xi_e}\sinh(2\xi_e)(\cosh(2\xi_e) + \cosh(2\xi_1))$$

$$- 4e^{2\xi_e}sinh^2(2\xi_e)\big\}2e^{2\xi}\cos 2\eta$$

$$+ \big\{2\sinh(2\xi_e)(\cosh(2\xi_e) + \cosh(2\xi_1))$$

$$- 2e^{-2\xi_e}sinh^2(2\xi_e)\big\}2e^{-2\xi}\cos 2\eta + 2\sinh(2\xi_e)\Big]$$

Using these components of stresses, we can evaluate Principal Plane Stress around the crack by using Von Misses Stress formulation.

$$\sigma = \sqrt{{\sigma_{\xi\xi}}^2 + {\sigma_{\eta\eta}}^2 - \sigma_{\xi\xi}\sigma_{\eta\eta} + 3{\sigma_{\xi\eta}}^2} \tag{3.23}$$

We define dimensionless form of these stress equation for convenience using following evaluation

$$\overline{\sigma_{\xi\xi}} = \frac{\sigma_{\xi\xi}}{\Delta P} = \frac{\sigma_{\xi\xi}}{P_e - P_w} \tag{3.24.1}$$

$$\overline{\sigma_{\eta\eta}} = \frac{\sigma_{\eta\eta}}{\Delta P} = \frac{\sigma_{\eta\eta}}{P_e - P_w} \tag{3.24.2}$$

$$\overline{\sigma_{\xi\eta}} = \frac{\sigma_{\xi\xi}}{\Delta P} = \frac{\sigma_{\xi\xi}}{P_e - P_w} \tag{3.24.3}$$

CHAPTER 4

RESULTS AND DISCUSSION

In dimensionless units, crack length of unit dimension is considered, with well opening at 0 and Crack tip at +/- 0.5 as shown in Figure (4.1).

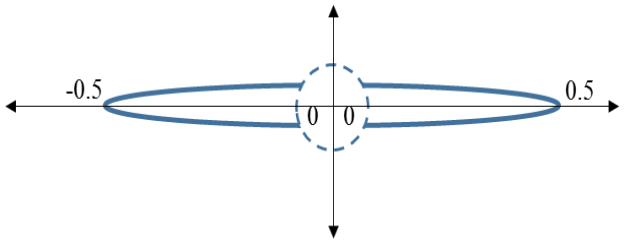

Figure 4.1 General View of the Fracture Domain as Used in Plots

Dimensionless stress values are evaluated using equations (3.24.1), (3.24.2), and (3.24.3) and are plotted for the better understanding of the stress distribution.

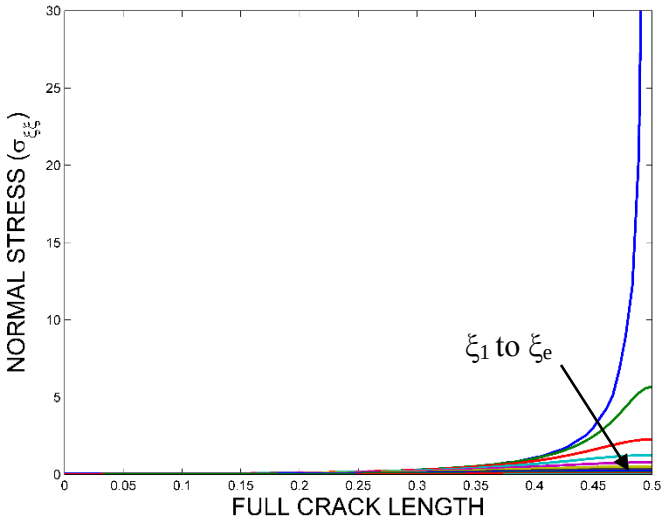

Figure 4.2 Normal Stress ($\overline{\sigma_{\xi\xi}}$) Distribution for Half Crack Length With $\xi_1 = 0.001$, $\xi_e = 5$, $C_{fd} = 5$

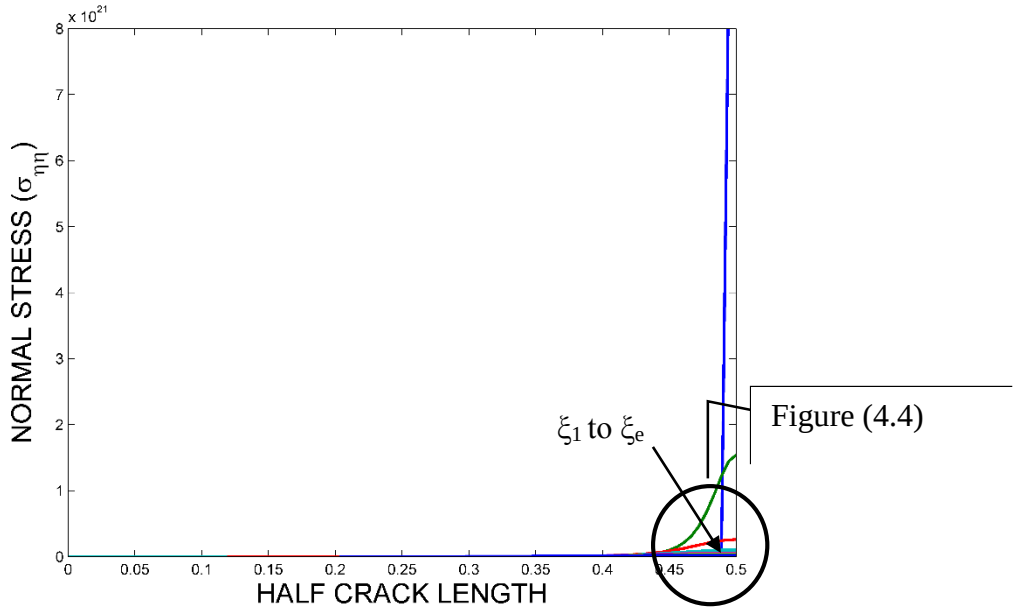

Figure 4.3 Normal Stress ($\overline{\sigma_{\eta\eta}}$) Distribution for Half Crack Length With ξ_1 = 0.001, ξ_e = 5, C_{fd} = 5

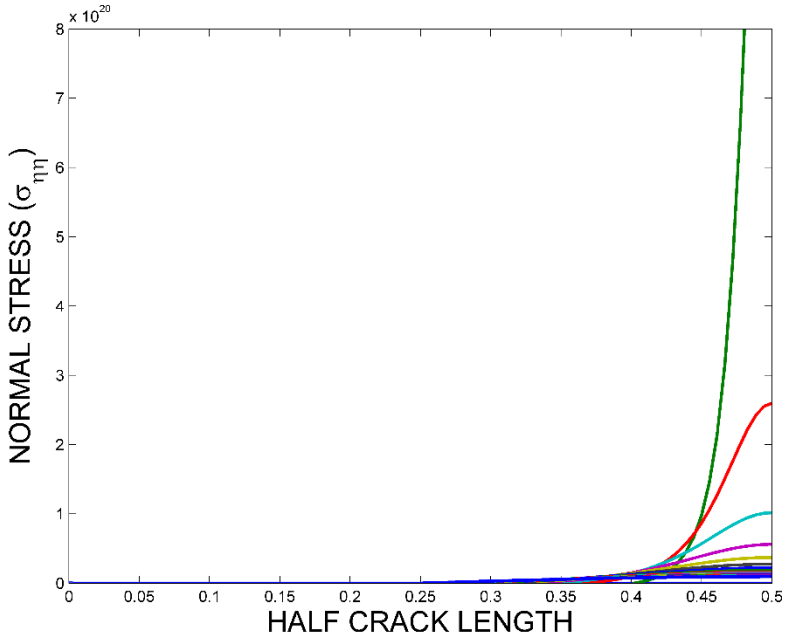

Figure 4.4 Zoom in View of Normal Stress ($\overline{\sigma_{\eta\eta}}$) Distribution for Half Crack Length With ξ_1 = 0.001, ξ_e = 5, C_{fd} = 5

It is clearly evident from Figure (4.2) & (4.3) that maximum stress appears on the fracture boundary. Stress values are almost linear and very low in the region away from the fracture surface. Since fracture closure is directly related to the stress acting on the fracture surface, we will focus on stress values at the fracture boundary i.e. at $\xi = \xi_1$.

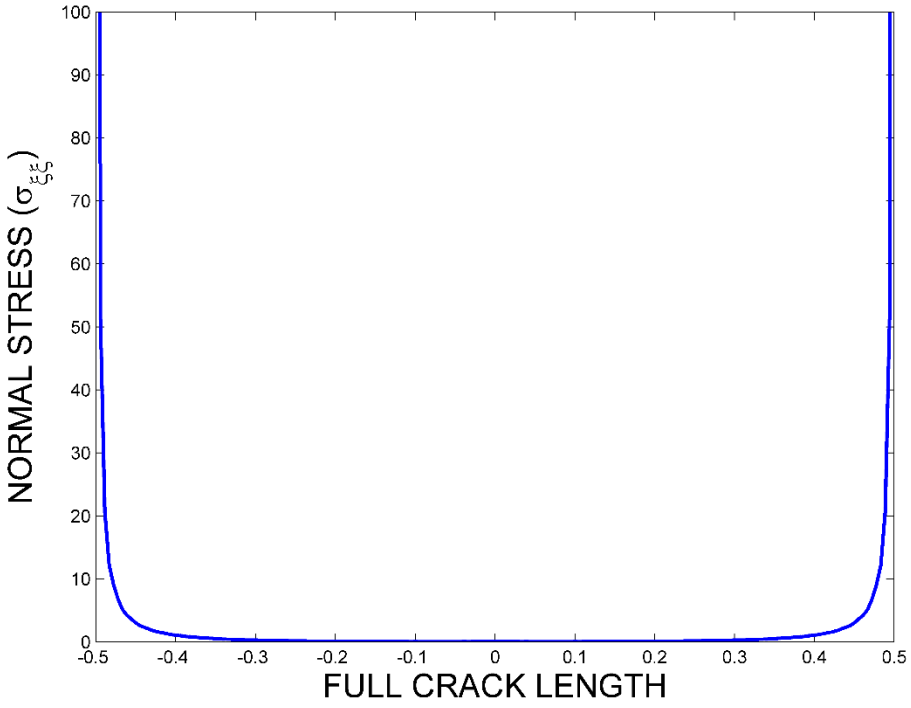

Figure 4.5 Normal Stress ($\overline{\sigma_{\xi\xi}}$) at Crack Boundary for Entire Crack Length With $\xi_1 = 0.001$, $\xi_e = 5$, $C_{fd} = 5$

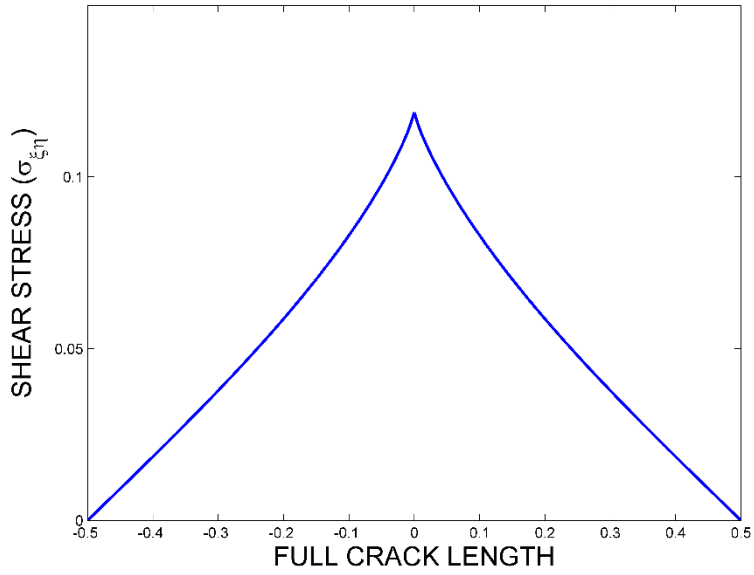

Figure 4.6 Shear Stress ($\overline{\sigma_{\xi\eta}}$) at Crack Boundary for Entire Crack Length With $\xi_1 = 0.001$, $\xi_e = 5$, $C_{fd} = 5$

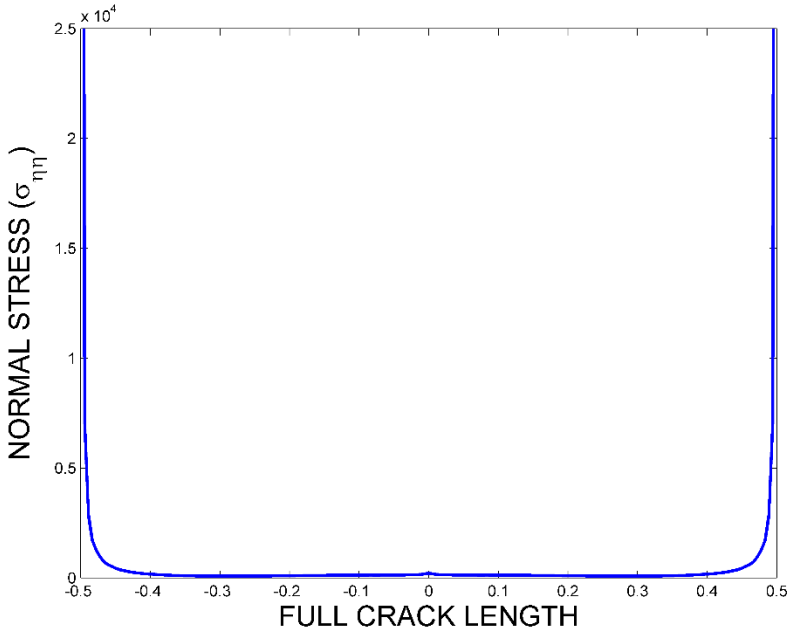

Figure 4.7 Normal Stress ($\overline{\sigma_{\eta\eta}}$) at Crack Boundary for the Entire Crack Length With $\xi_1 = 0.001$, $\xi_e = 5$, $C_{fd} = 5$

It is seen from the above plots that at the fracture boundary, there is very high hoop stress concentration at the fracture tip due to the high flux concentration caused by the pressure gradient singularity.

Results are evaluated at the crack boundary to determine the effects caused by stresses to the fracture. Since results are symmetrical along X axis and beyond $\pi/2$ (point '0' on X axis) crack is assumed to open at the well interface, from here on results are plotted only for half crack length for ease.

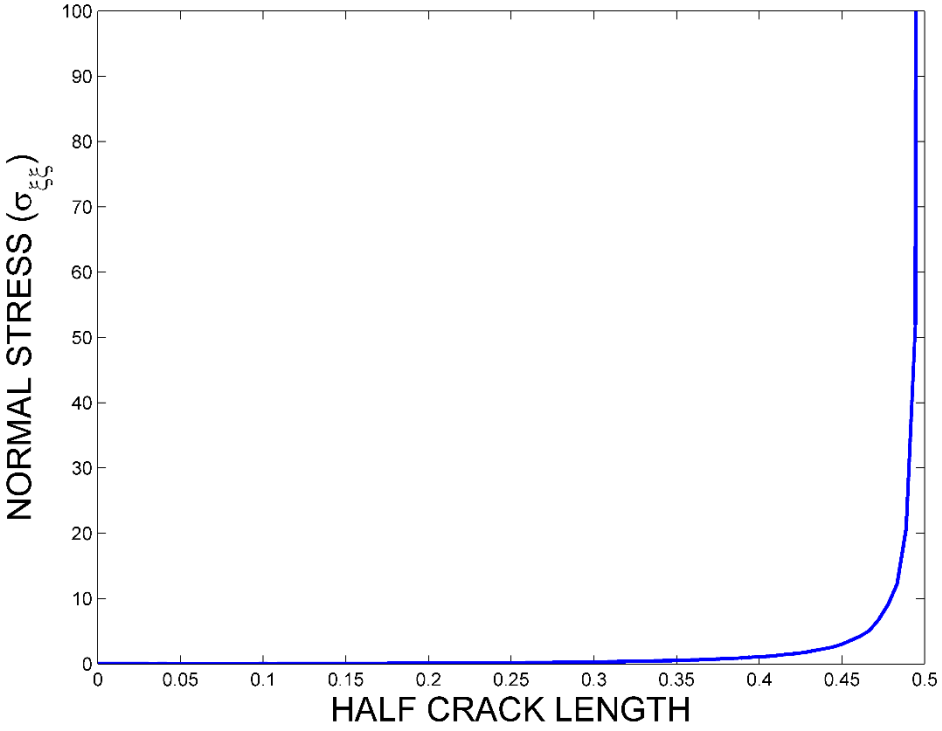

Figure 4.8 Normal Stress ($\overline{\sigma_{\xi\xi}}$) at Crack Boundary With $\xi_1 = 0.001$, $\xi_e = 5$, $C_{fd} = 5$

It is seen that Normal stress $\overline{\sigma_{\xi\xi}}$ generates negligible stress distribution along the fracture boundary but high stress concentration is observed at the tip.

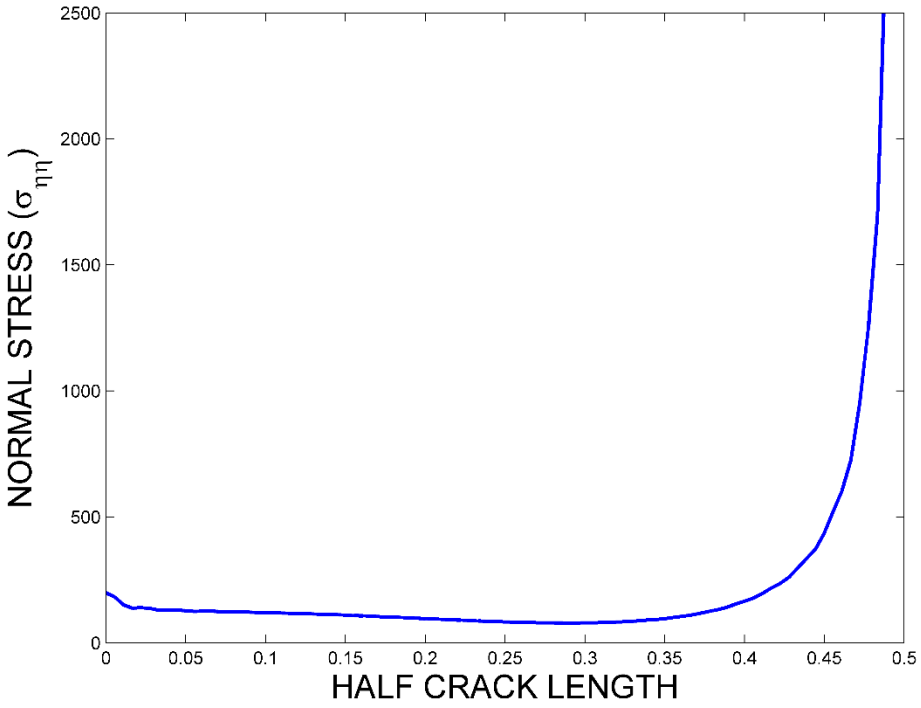

Figure 4.9 Normal Stress ($\overline{\sigma_{\eta\eta}}$) at Crack Boundary With $\xi_1 = 0.001$, $\xi_e = 5$, $C_{fd} = 5$

When dimensionless normal stress $\overline{\sigma_{\eta\eta}}$ (Hoop Stress) are plotted, it is seen that this normal stress also creates a very high concentration at the crack tip. Values of this normal stress in η direction are much higher than stresses in ξ direction.

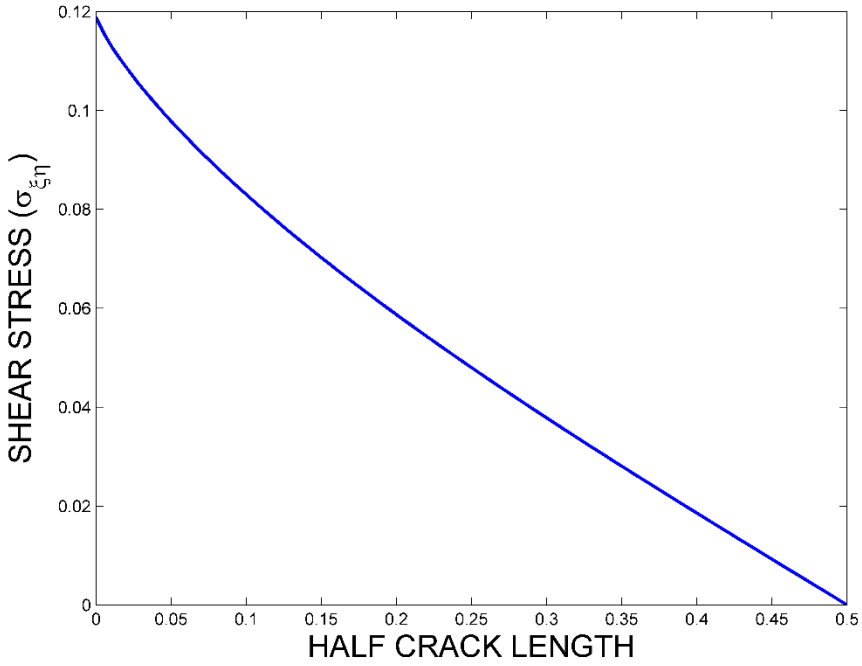

Figure 4.10 Shear Stress ($\overline{\sigma_{\xi\eta}}$) at Crack Boundary With $\xi_1 = 0.001$, $\xi_e = 5$, $C_{fd} = 5$

When shear stress is plotted along the boundary of the fracture, it is seen that shear stress does not vary much throughout the crack surface and thus does not have much effect on the stress concentration on the fracture.

When both the normal stresses are compared with each other as shown in Figure (4.11) at the fracture boundary, it is seen that $\overline{\sigma_{\eta\eta}}$ has extremely large value as compared to $\overline{\sigma_{\xi\xi}}$. This is caused due to 'Hoop Stress Effect'. This is an indication that crack may fail if the hoop stress is very high.

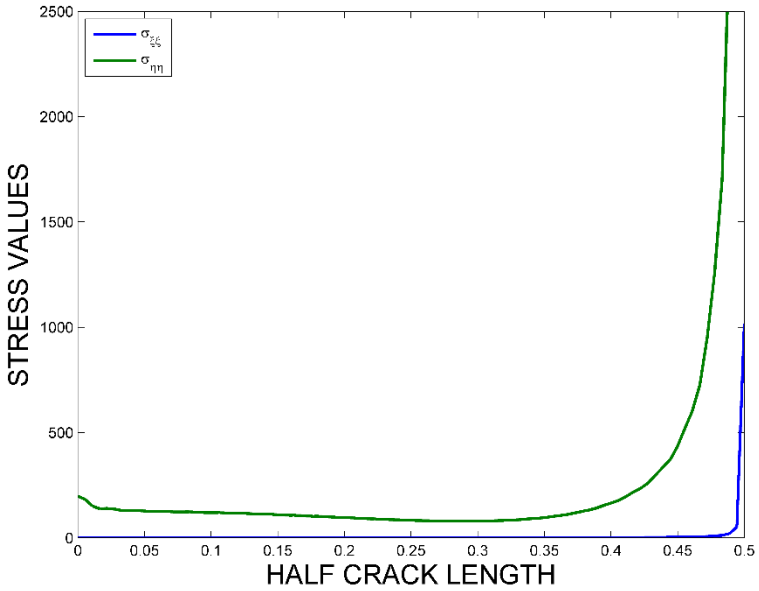

Figure 4.11 Comparison of Normal Stresses $\overline{\sigma_{\xi\xi}}$ and $\overline{\sigma_{\eta\eta}}$ at Crack Boundary With $\xi_1 = 0.001$, $\xi_e = 5$, $C_{fd} = 5$

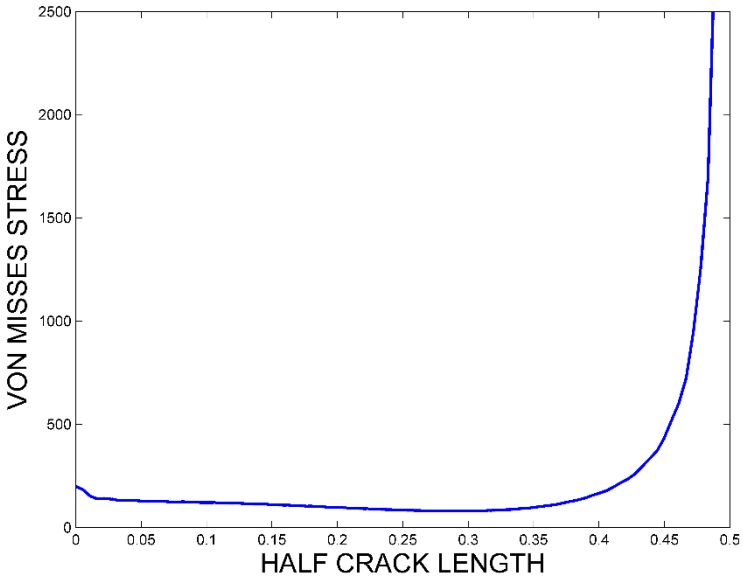

Figure 4.12 Von Mises Stress at Crack Boundary Showing Values From ξ_1 to ξ_e, With $\xi_1 = 0.001$, $\xi_e = 5$, $C_{fd} = 5$

Von Mises stress is plotted along with fracture boundary, which also indicates high stress concentration at the crack tip. These values are very critical to estimate whether the poroelastic soil medium around the well can withhold the stress generated due to the pressure induces force.

Different parameters affecting the high stress concentration are also studied. Plots are shown to study the effect of degeneration of the fracture, where ξ_1 is reduced to simulate the condition in which the fracture width is reduced and assumed that the fracture lies completely on X axis.

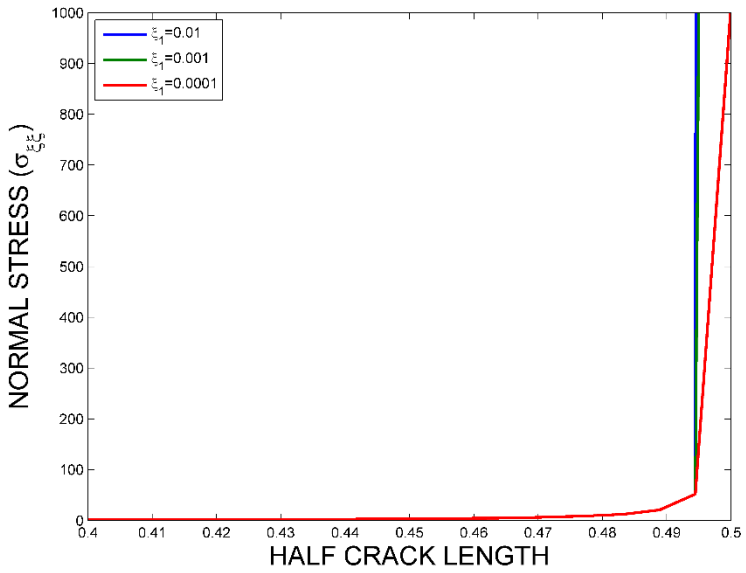

Figure 4.13 Comparison of Normal Stress ($\overline{\sigma_{\xi\xi}}$) at Crack Boundary With ξ_1 = 0.01, ξ_1 = 0.001 & ξ_1 = 0.0001

Figure (4.13) indicates that as fracture is made thinner i.e. ξ_1 is reduced further, Normal Stress concentration ($\overline{\sigma_{\xi\xi}}$) along the fracture reduces but higher stress concentration is seen at the crack tip.

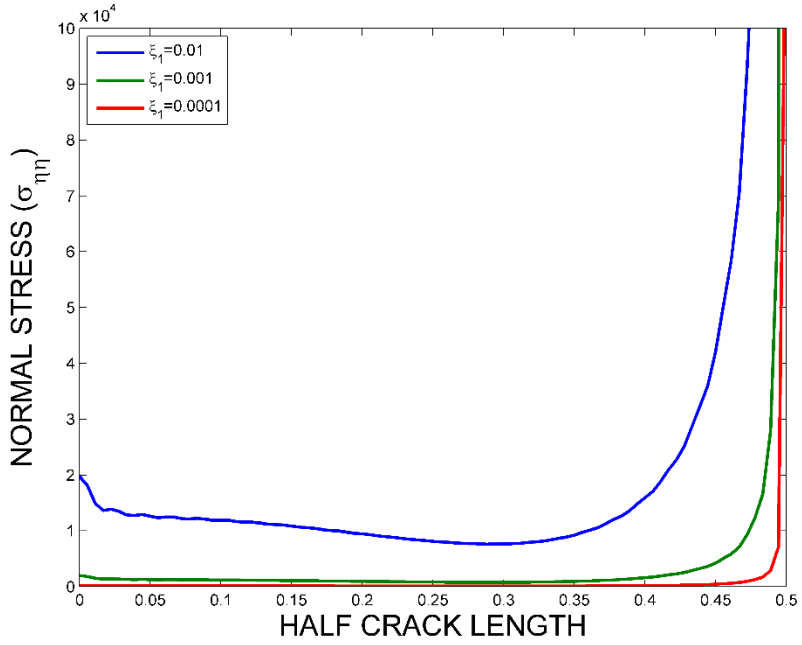

Figure 4.14 Comparison of Normal Stress ($\overline{\sigma_{\eta\eta}}$) at Crack Boundary With ξ_1 = 0.01, ξ_1 = 0.001 & ξ_1 = 0.0001

Figure (4.14) shows that as fracture is made thinner i.e. ξ_1 is reduced further, Normal Stress concentration ($\overline{\sigma_{\eta\eta}}$) increases very drastically at the crack tip and eventually will reach infinity as ξ_1 approaches 0.

Stress distribution for different values of fracture conductivity (C_{fd}) are also studied. When C_{fd} approached infinity, it indicates the maximum production that can be achieved through a wellbore for a given drawdown pressure.

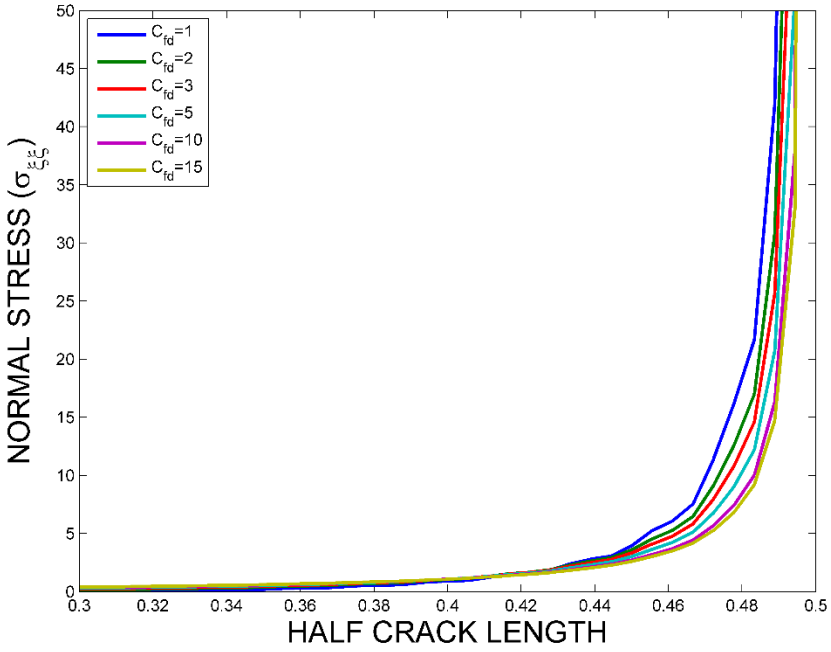

Figure 4.15 Comparison of Normal Stress ($\overline{\sigma_{\xi\xi}}$) With C_{fd} = 1, 2, 3, 5, 10 & 15, at Crack Boundary With ξ_1 = 0.001

It is seen from Figure (4.15) that as the C_{fd} values are increased, the stress distribution reduces along the fracture length but higher stress concentration are observed at the fracture tip for very high C_{fd} Values.

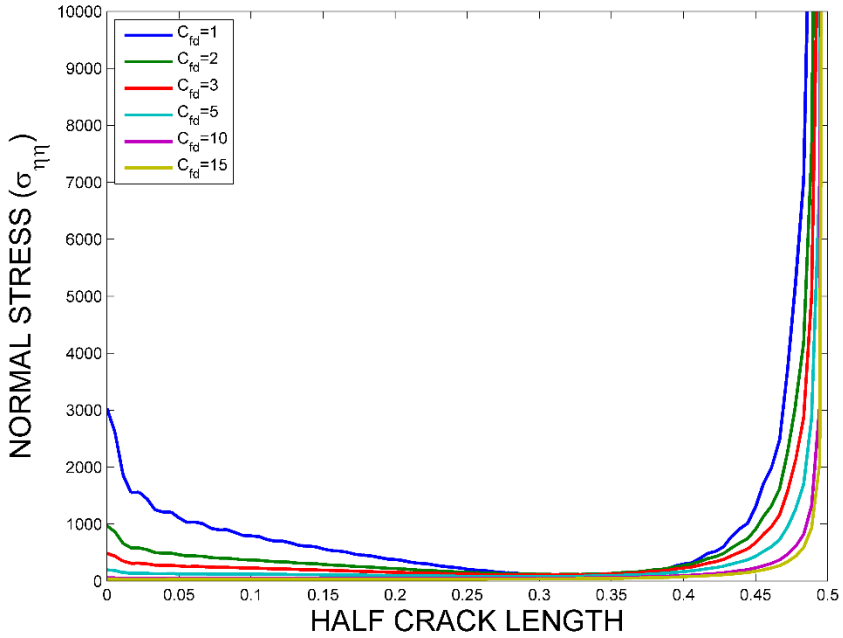

Figure 4.16 Comparison of Normal Stress ($\overline{\sigma_{\eta\eta}}$) With C_{fd} = 1, 2, 3, 5, 10 & 15, at Crack Boundary With ξ_1 = 0.001

It is seen from Figure (4.16) that, when the C_{fd} values are increased, stress distribution along the crack length decreases but at the crack tip high values of stresses are achieved. This is caused due to the pressure gradient singularity effect causing suction at the crack tip, thus increasing the flow production.

Similarly stress distribution due to increasing outer boundary value is also studied for a constant C_{fd} value.

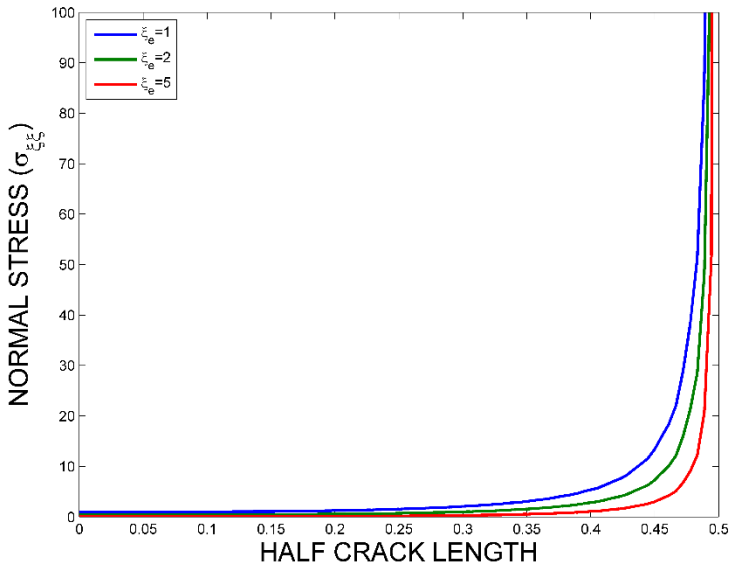

Figure 4.17 Comparison of Normal Stress ($\overline{\sigma_{\xi\xi}}$) With ξ_e =1, ξ_e =2, ξ_e =5 Increasing in the Direction of the Arrow Withξ_1 = 0.001, C_{fd} = 5, at Crack Boundary

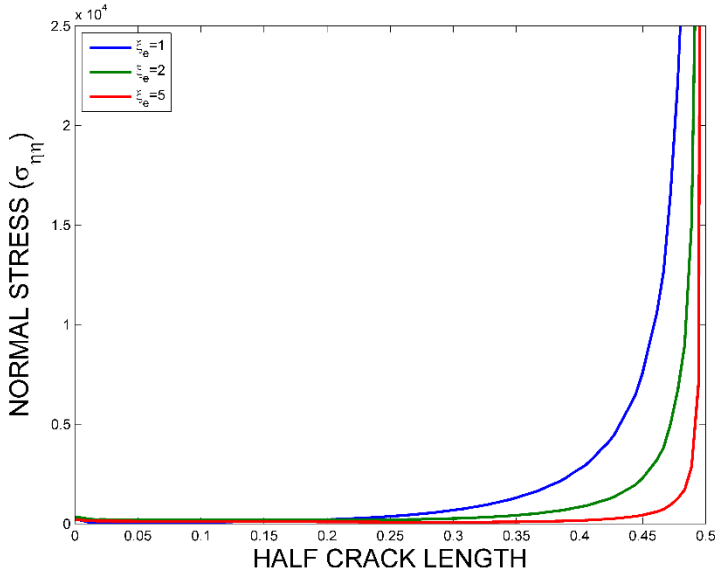

Figure 4.18 Comparison of Normal Stress ($\overline{\sigma_{\eta\eta}}$) With ξ_e =1, ξ_e =2, ξ_e =5 Increasing in the Direction of the Arrow With ξ_1 = 0.001, C_{fd} = 5, at Crack Boundary

From Figure (4.17) it is seen that as the far end boundary is increased even further, the normal stress distribution $\overline{\sigma_{\xi\xi}}$ flattens out giving very low linearly distributed value of stress.

From Figure (4.18), it is seen that for a constant fracture conductivity, stress distribution along the crack length decreases with increase in the far end boundary except for the crack tip where the stress values increases drastically showing almost singular behavior.

CHAPTER 5

CONCLUSION AND FUTURE WORK

(1) It is clearly seen from Figures (4.2) and (4.3) that there is high stress concentration at the fracture boundary due to the pressure induced flow. Figure (4.7) shows that even though there are low tensile stress values along the fracture, high stress concentration is seen at the crack tip, where pressure gradient singularity is found to be occurred by Chen et al (2014). This shows that pressure gradient singularity causes very high stress values even for finite conductivity of the fracture. This in turn affects the closure stresses.

(2) Figure (4.8) & (4.10) indicates that there is almost negligible shear stress effect even along the fracture boundary.

(3) Figure (4.11) shows that the normal stress in η direction is much higher than the normal stress in ξ direction, indicating that hoop stress effect due to the pressure gradient singularity at the crack tip is very prominent. Even though it has been shown by Warpinski et. al. (1998) that crack closure is a slow process, it ultimately stops the well production. So to encounter this loss in the production, stresses caused by fluid production needs to be considered in well stimulation approaches.

(4) Figure (4.13) & (4.14) indicates that as the ellipse for the fracture is made thinner overlapping the X axis, hoop stress distribution along the crack decreases with less area covered, but the value of stress concentration at the crack tip increases drastically.

(5) Figure (4.15) & (4.16) shows that as the conductivity increases, the stress concentration at the tip also increases and the stress value at the crack tip becomes singular as conductivity approaches infinity. This is in accordance with the research shown by Chen et al (2014)

(6) All this results indicates that there is certainly very high hoop stress concentration at the fracture tip caused due to the pressure induced flow. So further investigation needs to be done to reevaluate the Closure Stress Values considering the Stress effects due to fluid production. This will help in developing better proppants and injection techniques thus allowing more and prolonged production rate from the well.

REFERENCES

Barber J. R. (2002), 'Elasticity', Second Edition, eBook ISBN: 0-306-48395-5

Biot. M. A. 'General theory of three-dimensional consolidation', J. Appl. Phys., 12. 155. 1941.

Chen K. P., Yan Jin & Mian Chen 2013, 'Pressure-gradient singularity and production enhancement for hydraulically fractured wells', Geophys. J. Int. (2013) 195, 923–931

Chen K. P., Yan Jin, Mian Chen, 'Analytical Solution and Mechanisms of Fluid Production from Hydraulically-fractured Wells with Finite Fracture Conductivity'

Chow W. T., S. N. Atluri (1995), 'Finite element calculation of stress intensity factors for interfacial crack using virtual crack closure integral', Computational Mechanics November 1995, Volume 16, Issue 6, pp 417-425

Coker, E. G, Filon, L. N. G, (1957), 'A Treatise on Photo-Elasticity'

Elizabeth Ritz, David D. Pollard (2011), 'Closure of circular arc cracks under general loading: effects on stress intensity factors', Int J Fract (2011) 167:3–14

Fjær E., R.M. Holt, P. Horsrud, A.M. Raaen & R. Risnes, (1992) 'Petroleum Related Rock Mechanics (Second Edition)'

Gidley, J.L., Holditch, S.A., Nierode, D.E. et al. 1989. Rock Mechanics and Fracture Geometry. In Recent Advances in Hydraulic Fracturing, 12. Chap. 3, 57-63. Richardson, Texas: Monograph Series, SPE.

Gidley, J.L., Holditch, S.A., Nierode, D.E., and Veatch, R.W. Jr. (1989), 'Recent Advances in Hydraulic Fracturing', SPE Monograph Vol. 12, Society of Petroleum Engineers, Richardson, Tex.

Gringarten, A. C., Ramey, H. J., Jr. & Raghavan, R., 'Applied pressure analysis for fractured wells.' J. Pet. Technol., 27(7), 887–892, 1975.

Huston Ronald, Josephs Harold, (2009), 'Practical Stress Analysis in Engineering Design', Third Edition, ISBN: 978-1-57444-713-2

Maiti S. K, N. K. Mukhopadhyay, A. Kakodkar (1997), 'Boundary element method based computation of stress intensity factor by modified crack closure integral', Computational Mechanics 19 (1997) 203 – 210 O Springer-Verlag 1997

Montgomery, C.T., and Steanson, R.E., 'Proppant Selection—The Key to Successful Fracture Stimulation (Revised),' Paper No. SPE 12616, SPE Deep Drilling and Production Symposium and Technical Exhibition, Amarillo, Tex., Apr. 1-3, 1984.

Muskhelishvili N (1953) Some basic problems of the mathematical theory of elasticity. P. Noordhoff Ltd, Groningen, Holland

Prats, M. 1961, Effect of vertical fractures on reservoir behavior-incompressible fluid case. SPE J. 1(2), 105-118.

Prats, M., 'Effect of vertical fractures on reservoir behavior-compressible fluids case.' SPE J. 1(2), 105-118, 1961.

Prats, M., Hazebroek, P., & Strickler, W. R, 'Effect of vertical fractures on reservoir behavior-compressible fluids case.' SPE J. 2(2), 87-94, 1962.

Ratts, P.A.C. 2007, Uptake of water from soils by plant roots. Transp. Porous Med. 68:5–28.

Roose, T. & Schnepf, A. 2008, Mathematical models for plant-soil interaction. Phil. Trans. R. Soc. A, 366, 4597-4611.

Sookprasong, P.A., 'Plot procedure finds closure pressure', OGJ, Sept. 8, 1986, pp. 110-12.

Sookprasong, P.A., (2010), 'In situ Closure Stress on Proppant in the Fracture, a Controversial New Thinking'

Sung Pil Heo, Won Ho Yang, Cheol Kim (2002), 'Stress Intensity Factors for Elliptical Arc Through Cracks In Mechanical Joints by Virtual Crack Closure Technique', KSME International Journal. Vol. 16 No.2, pp. 182-191, 2002

Warpinski, N.R., Peterson, R.E., Branagan, P.T., Wolhart, S.L. (1998). 'In situ stress and moduli: Comparison of values derived from multiple techniques'. SPE 49190. In: SPE Ann. Tech. Conf. & Exh., Louisiana, September 27–30.

[1] http://www.slb.com/resources/publications/oilfield_review/~/media/Files /resources/ oilfield_review/ ors13/sum13/ defining_hydraulics.ashx